Supplemental Information

MAL3 MASKS CATASTROPHE EVENTS IN *SCHIZOSACCHAROMYCES POMBE* MICROTUBULES BY INHIBITING SHRINKAGE AND PROMOTING RESCUE

Miho Katsuki, Douglas R. Drummond, Michael Osei, and Robert A. Cross

Table of Contents:

SUPPLEMENTAL METHODS:

Preparation of polarity marked seeds

To exclude potential cross contamination, microtubules in our assay were nucleated from seeds containing only tubulin, rather than from axoneme fragments or centrosomes. To make polarity-marked pig GMPCPP-microtubule seeds, a core segment was first polymerised by incubating 30 µM of pig tubulin with 10% Alexa 488-labelled pig tubulin heterodimers in PEM buffer (100 mM Pipes, pH 6.9, 1 mM $MgSO_4$ and 2 mM EGTA) (1) containing 1mM GMPCPP at 37 °C for 1 hr. Next the core segment solution was diluted 1:40 by volume into the elongation solution containing 11 µM of pig brain tubulin with 93.6% Alexa 680-labelled pig tubulin heterodimers, 0.5 mM GMPCPP and 1 mM DTT in BRB (80 mM Pipes, pH 6.8, 1 mM $MgCl_2$, 1 mM EGTA), and incubated at 37 °C for 1hr. The seeds were kept at 25 °C during experiments. In these conditions, the seeds were about 5 – 20 µm in length.

Motility assay to determine seed polarity

Microtubule seed polarity was confirmed by gliding assay using rat kinesin-1 construct K430-GST (2). K430GST (stock concentration, 11.5 µM) was diluted to 5.75 µM in BRB buffer before loading into the assay chamber, incubated for 5 min and the chamber then rinsed with 40 µl of BRB buffer. Polarity-marked pig GMPCPP-microtubule seeds were loaded into the chamber in BRB buffer supplemented with 1 mM Mg-ATP, 1 mM DTT, 0.1 mg/ml BSA and an oxygen scavenger system (8 µg/ml catalase, 4.5 mg/ml glucose, 38 unit/ml glucose oxidase and 1% (v/v) 2-mercaptoethanol) and microtubule sliding observed using fluorescence microscopy at 25 °C. In this assay, 100% of seeds moved with 83% having the longer Alexa-680 tubulin labelled region at the trailing microtubule plus end (Supplemental Movie, movie1.mov).

Microtubule dynamics assay

A Sigma-cote (SL-2, Sigma) coated coverglass was attached to a slideglass by double-sided sticky tape (dimensions 18 mm × 6 mm × 82 µm). The flow-chamber was treated first with 10% (v/v) anti-Alexa 488 antibody (A11094, Invitrogen) in PEM buffer for 5 min, then excess anti-body was washed out with 4 volumes of PEM buffer. 2 volumes of 0.1 mg/ml of casein in PEM buffer was flowed in and incubated for 5 min then washed by 4 volumes PEM buffer. 2 volumes of polarity-marked microtubule seeds diluted 50x in PEM buffer were flushed into the flow cell and allowed to adhere to the glass surface for 5 min. After flushing the non-attached microtubule seeds from the chamber using 4 volumes of PEM buffer, 4

volumes of 4.5 μM non-labelled *S. pombe* single isoform tubulin in PEM buffer containing 1 mM GTP, 1 mM Mg-ATP, 1 mM DTT and an oxygen scavenger system (8 μg/ml catalase, 4.5 mg/ml glucose, 38 unit/ml glucose oxidase and 1% (v/v) 2-mercaptoethanol) was flowed in. These conditions produce dynamic instability events at convenient intervals (Fig. 1C). Assays were also done with the addition of different concentrations of unlabelled Mal3. Flow cells were incubated for 25 min at 25 °C to achieve steady state before imaging microtubule dynamics for a further 30 min by dark-field illumination, We found that microtubule dynamics were unaltered by continuous observation for half an hour or more under full intensity illumination using the 546 nm spectral line of the 100W mercury lamp (Fig. 1C).

Imaging

Dynamic microtubules were imaged using dark-field microscopy, which avoids the need for fluorescent labelling of proteins, thereby removing any concern that tagging with a large fluorophore might in some way alter function, and the related potential for fluorophore-mediated photodamage of the proteins. Dark-field illumination also produces a high-contrast white-on-black image of the microtubule tip even when the tip is far from the surface. This avoids the requirement in total internal reflection fluorescence (TIRF) microscopy that microtubules be constrained within the shallow excitation zone of about 100 nm immediately adjacent to the coverslip. The high contrast dark-field image of non-labelled microtubules is also suitable for automated image analysis (Fig. 1C, D).

A Nikon E800 microscope with a Nikon Plan Fluor x100 0.5-1.3 variable (iris) objective lens and x 1.25 intermediate magnification was used. Images were captured using an electron-multiplying CCD camera (Andor, iXon^{EM}+ DU-897E) and 100 ms exposures at 1 Hz for dynamic *S. pombe* microtubules by dark-field illumination and 200 ms exposures at 0.0167 Hz for microtubule seeds by epifluorescence during a 30 minute period with Metamorph software (Molecular Devices) for microscope control and image capture.

Epifluorescence imaging of Alexa-488 and Alexa-680 labelled microtubule seeds used E460SPUVv2 excitation and D525/20m emission filters for Alexa-488, and S654/24x excitation and S710/60m emission filters for Alexa-680 (Chroma). Filters were mounted in motorised filterwheels, (LEP MAC5000) with a further wheel providing ND filter control of excitation intensity from a 100W mercury lamp. A FF502/670-Di01 dichroic mirror (Semrock) that allows simultaneous epifluorescence and dark-field imaging was mounted in a customised Nikon filter cube. Shutters in the epi and Dia illumination paths allowed switching between epifluorescence and dark-field imaging.

Dark-field imaging of unlabelled microtubules used a Nikon dark field 1.43 – 1.20 NA oil condenser. Illumination was by a 100W mercury lamp connected to the microscope via a fibre optic light scrambler incorporating a cold mirror to remove both UV and IR wavelengths (Technical video). A custom made coupling was used to enable full illumination of the dark-field condenser back aperture. A GIF bandpass filter (500–568 nm, Nikon) centred on the 546 nm mercury lamp emission line attenuated wavelengths that would excite the Alexa fluorophores.

The entire microscope was enclosed in a custom built box with an incubator air heating system (Stuart), which maintained the temperature at 25 ± 0.5 ^{o}C.

Image analysis

A custom macro was written for the program ImageJ (Rasband, W.S., ImageJ, U. S. National Institutes of Health, Bethesda, Maryland, USA, http://rsb.info.nih.gov/ij/, 1997-2009) to automatically identify and digitize the microtubule end position in the kymographs of dynamic microtubules. The kymograph slice corresponding to each time point was analysed separately. The standard deviation (SD) of the intensity values within a 0.64 μm window along the microtubule length axis was calculated. The window centred over the microtubule tip has the biggest SD of grey values because of the difference between the high intensity dark-field microtubule image and the low background values. The middle point of the data window with the biggest SD was defined as the microtubule end.

Superimposing and aligning catastrophe events

For each Mal3 concentration data points from multiple catastrophe events were superimposed, aligned, and filtered to reduce noise and enable analysis of the transition kinetics of the events.

Catastrophe events were identified which had a growth phase equal to or greater than 47 sec before the catastrophe event and a shrinkage phase of at least 9 sec after the catastrophe event. Analysis of the growth and shrinkage rates from these events showed that they were typical of the entire population of events (Supplemental Table I). Best-fit lines of the growth and shrinkage phases were determined by linear regression and the intersection of the lines used as an initial estimate of the catastrophe event centre, which was set as the origin. The primary data points between -48 to +10 pixels corresponding to -48 to +10 seconds along the X axis were selected and excised. A custom VBA macro for Excel (Microsoft) was used to determine the optimum alignment of the catastrophe events using a shuffling algorithm that minimises the absolute deviation between the data points of each data set, combines the aligned data sets and determines the median length measurement for each timepoint.

In detail the macro uses the data points of catastrophe event 1 as template1 and places its origin at the centre of a 9x9 grid of pixels. The event data points are plotted relative to the origin with X axis (time) values rounded to integers. The origin of event2 is then placed in each pixel of the 9x9 grid in turn. For each position (a total of 81 positions) the absolute difference in Y axis position (Mt length) between event1 and event2 along the grid is summed. The minimum value of the sum of absolute displacements gives the best alignment of the two data sets. The procedure is then repeated comparing all the events in turn to template1. The data sets are then combined in their best alignments to event1 and the median Y (length) value determined for each X (time position). These median values are now used as template2.

Using template2 the procedure is repeated comparing all the event data sets in turn to template2 to determine the best alignment. The median values of the new data alignment are now template3. The sum of the absolute difference between the template3 and template2 data at each time point in the grid is calculated.

The procedure is repeated generating new templates until the sum of the absolute differences between the last two templates is less than 0.1 pixels. This required between 4 and 17 iterations to converge upon a best-fit alignment of the catastrophe events.

The super-imposed and median filtered data sets were fitted by linear regression of the growth and shrinkage phases using Prism software (GraphPad Software, Inc). Prediction bands, which contain 95% of the data points for either the growth or shrinkage phases were plotted using Prism. These prediction bands define the data points that belong exclusively to either growth or shrinkage with 95% probability. Other data points within the overlap region could belong to either growth or shrinkage or an additional transition. These were excluded from the analysis and the linear regression refitted with the remaining data points.

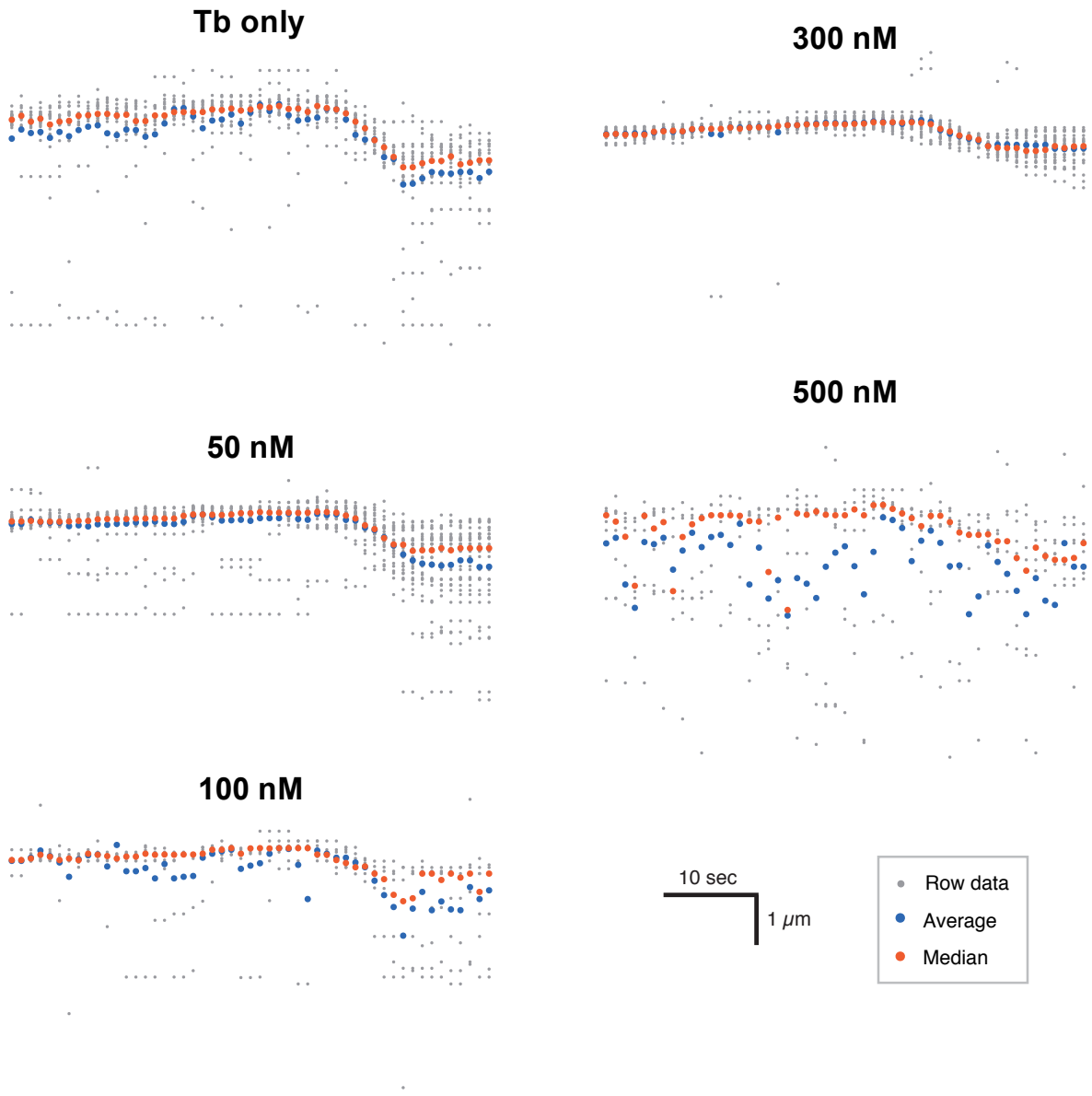

Figure S1 Comparison between averaging and median filtering. The grey dots indicate the super-imposed data points determined by the algorithm. Blue dots indicate the average and red the median value of the data at each time point. The median filter is better at removing the outlying data points, which often arise from lateral movement of the microtubule away from the line used to select the pixels for the Kymograph and are therefore more frequently found at positions corresponding to short lengths.

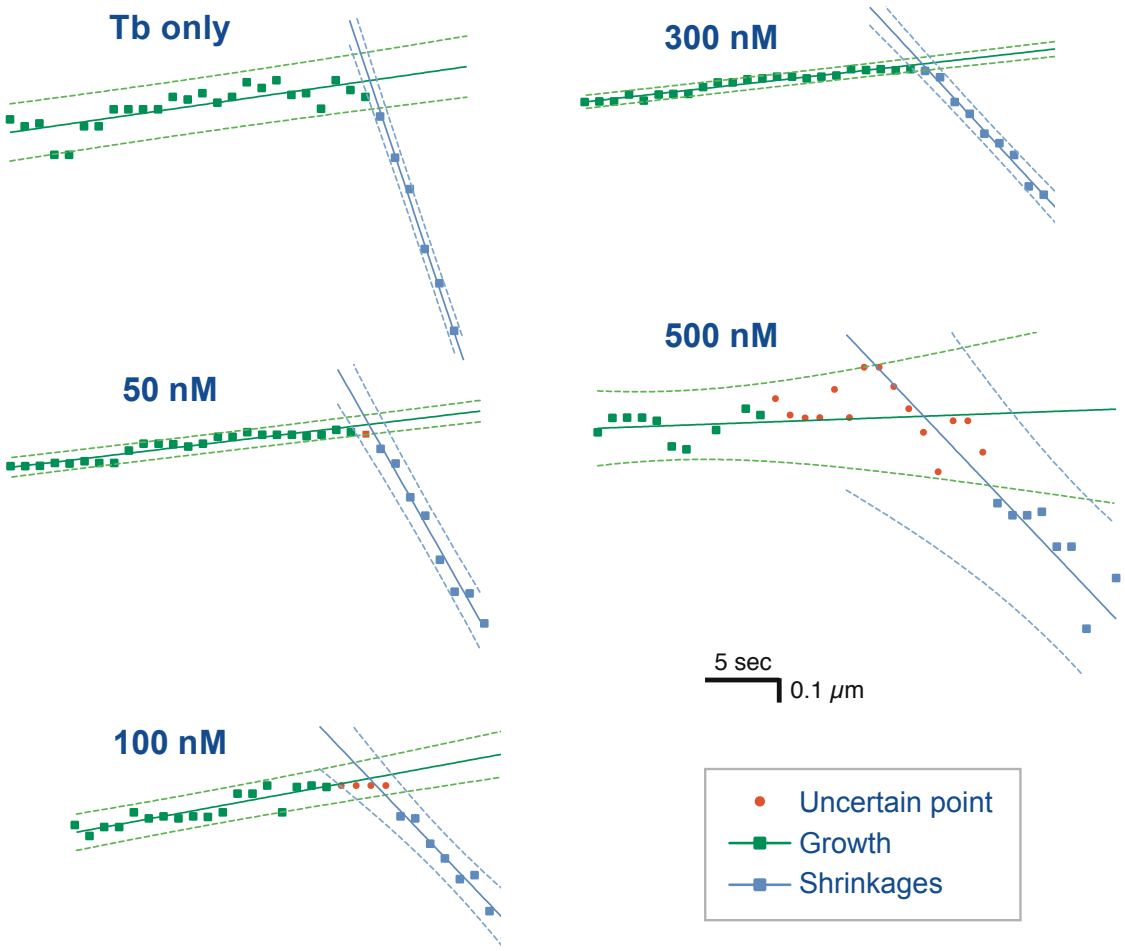

Figure S2 The uncertainty of growth or shrinkage at catastrophe. The data points predicted as only within the growth phase are indicated by green squares. The linear regression line and 95% prediction bands (enclosing 95% of data points) are shown by a green solid line and broken lines, respectively. For shrinkage, the data points and fitted lines are coloured blue. The points not uniquely assigned to either growth or shrinkage are shown in red.

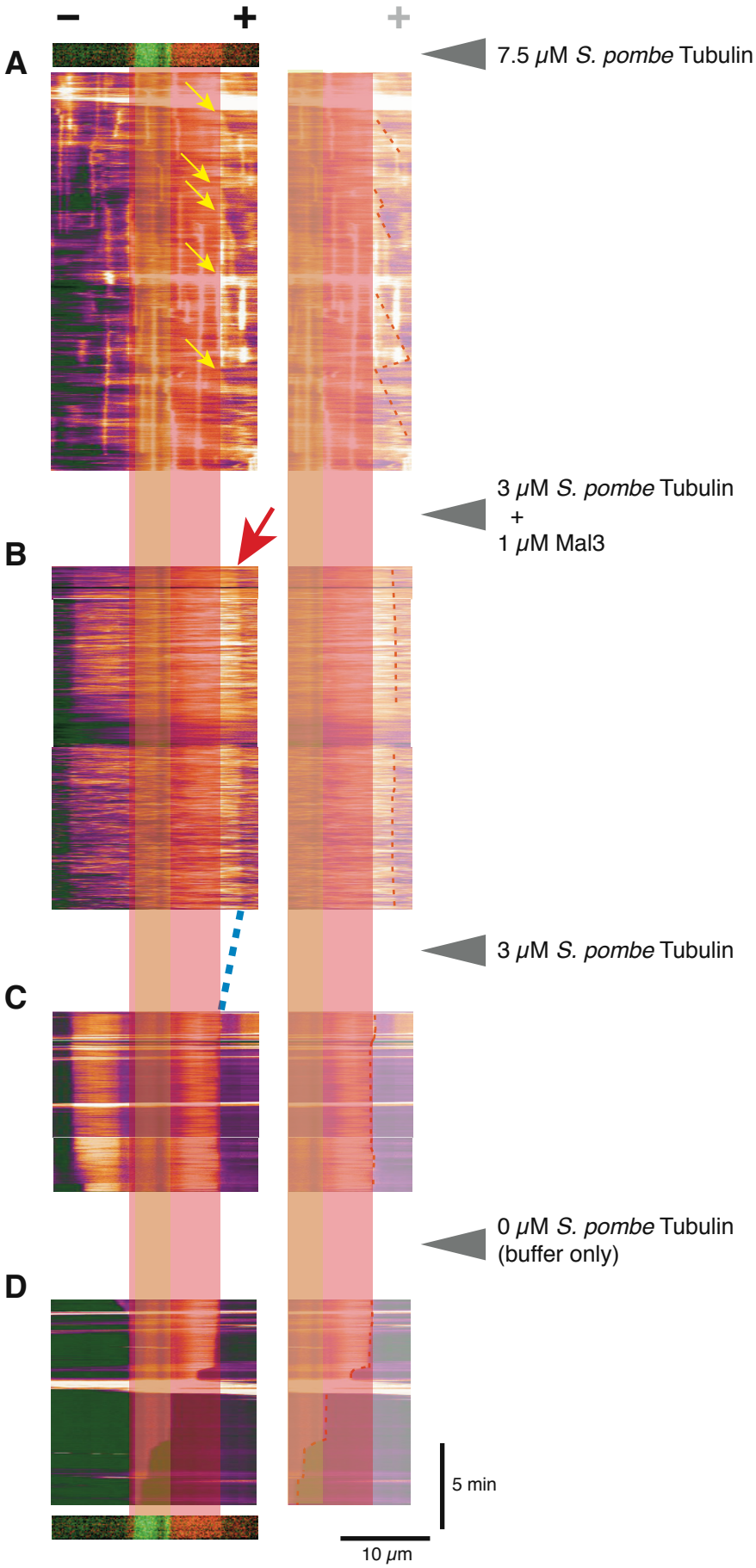

Figure S3 A high concentration of Mal3 stabilises microtubule plus end dynamics. Kymograph of microtubule dynamics in the presence of 7.5 μM of single isoform *S. pombe* tubulin (A). The flow chamber was then flushed out with 3 μM of *S. pombe* tubulin and 1 μM of Mal3 and the microtubules recorded (B). The chamber was then flushed out by 3 μM of *S. pombe* tubulin and the dynamics recorded (C) before finally flushing the chamber with PEM buffer (D). The kymograph image is duplicated in the right hand panel with the microtubule end positions traced by lines of red dots. At (A) the microtubule remains dynamic and the shrinking microtubule reaches the GMPCPP-seed (yellow arrows) however after reducing the tubulin concentration with Mal3 present the microtubules enter a paused state with no growth or shrinkage (red arrow). (B). Flushing with tubulin alone at low concentration causes depolymerisation of the microtubules back to the stabilised seed (C, blue dot line) and final flushing with buffer alone causes even the GMPCPP stabilised seed to depolymerise (D). The high tubulin concentration used to initially assemble the long *S. pombe* microtubules causes spontaneous nucleation in solution giving a high background in the dark-field images.

SUPPLEMENTAL TABLE 1

Microtubule dynamic parameters of the selected data set for superimposing
Data shows mean ± SD. n represents the number of events used for superimposing in Fig. 2B.

Plus end

Mal3 (nM)	0	50	100	300	500
Growth rate (μm/min)	0.53 ± 0.11 n = 20	0.51 ± 0.11 n = 32	0.48 ± 0.16 n = 8	0.62 ± 0.23 n = 26	0.46 ± 0.14 n = 9
Shrinkage rate (μm/min)	11.6 ± 4.1 n = 20	10.5 ± 4.7 n = 32	8.3 ± 4.6 n = 8	5.3 ± 1.7 n = 26	3.6 ± 1.2 n = 9

SUPPLEMENTAL REFERENCES:

1. Walker, R. A., O'Brien, E. T., Pryer, N. K., Soboeiro, M. F., Voter, W. A., Erickson, H. P., and Salmon, E. D. (1988) *J. Cell Biol.* **107**, 1437-1448
2. Crevel, I. M., Lockhart, A., and Cross, R. A. (1997) *J. Mol. Biol.* **273**, 160-170

LEGENDS FOR SUPPLEMENTAL MOVIES:

movie1.mov: Sliding assay of dual-coloured polarity marked microtubules. Alexa 488-marked microtubule segment is shown in green and Alexa 680-marked microtubule segment is shown in red. Scale bar : 20 μm. Top right of movie shows time in seconds. The field of view is changed at about 190 seconds.

movie2.mov: *S. pombe* microtubule dynamics assay in the absence of Mal3. Polarity-marked GMPCPP-microtubules are indicated by green and red as in movie1.mov. Dynamic non-labelled *S. pombe* microtubules are observed by dark-field illumination (microtubules are shown as white on black background). Microtubule polarity is indicated by "+" and "-". Scale bar : 5 μm. Top right of movie shows time in seconds.

movie3.mov: *S. pombe* microtubule dynamics assay in the presence of 300 nM Mal3. Microtubule polarity is indicated by "+" and "-". Scale bar : 5 μm. Top right of movie shows time in seconds. At this concentration Mal3 causes spontaneous polymerisation of *S. pombe* microtubule in solution. However this did not affect the measured growth rate showing an insignificant reduction in the free tubulin concentration in the assay.